

Stress rates in the central Cascadia subduction zone inferred from an elastic plate model

Charles A. Williams and Robert McCaffrey

Rensselaer Polytechnic Institute, Troy, New York

Abstract. GPS vectors and surface tilt and uplift rates from northwestern Oregon and southwestern Washington are inverted to estimate rates of stress changes along the Cascadia thrust fault and base of the overriding plate using a finite thickness elastic plate model. The data are fit by elevated shear stress and Coulomb Failure Function (CFF) rates within 80 km of the trench. By contrast, an elastic half-space dislocation model does not fit as well and predicts significant amounts of locking and elevated CFF rates near the coast.

1. Introduction

A primary motivation for collecting geodetic data during interseismic periods at subduction zones is the determination of the seismic hazard potential on the plate-bounding fault. Elastic half-space dislocations (EHSD) [Okada, 1985] have been successful in matching geodetic observations, from which the distribution of locking on the fault is inferred. Recent inversions of data from Oregon [McCaffrey *et al.*, 2000] using EHSD resulted in apparent locking of the plate-bounding fault both onshore and offshore, with an unlocked zone between. Those authors suggested that the zone of locking onshore may be due to the treatment of the base of the lithosphere in EHSD as a no-slip boundary, resulting in unrealistically high resistance of the lithosphere to trench-normal contraction. To investigate this and to evaluate the utility of EHSD during interseismic periods, we present an alternative model that considers a finite thickness overriding plate driven by stress rates along the fault boundary and base of the plate. We obtain a better fit to geodetic data from northern Oregon and fault locking below onshore regions is not required.

2. A finite plate model

Our model domain is an elastic layer in the shape of the overriding plate (Figure 1). Rather than explicitly including the subducting slab, we consider the stress changes transmitted by this slab to the overriding plate along the dipping thrust, consisting of shear stresses directed along dip and normal stresses perpendicular to the fault. Similarly, the asthenosphere transmits shear and normal stresses to the base of the plate. We use a modified version of a finite element code [Melosh and Raefsky, 1980] to compute synthetic Green's functions that give the displacements along the boundaries due to unit stresses applied at each of the nodes along the fault and base of the plate. Gravity is sim-

ulated by Winkler restoring forces [Williams and Richardson, 1991], and zero-displacement boundary conditions at infinity use the mapped infinite element technique [Bettess, 1992; Williams and Wadge, 1998]. Using the response functions we perform a linear least-squares inversion of surface geodetic data to solve for the distribution of stresses along the fault and base of the overriding plate. We use either triangular or Gaussian amplitude envelopes, step-ramp functions, or Chebyshev polynomials [Press *et al.*, 1992] to represent the stress distributions and use a genetic algorithm [Carroll, 1999] to optimize a fitness function that includes the condition of the inversion matrix [Curtis and Snieder, 1997], the normalized χ^2 misfit ($\chi_n^2 = \chi^2 / \text{number degrees of freedom}$), and the fit to the equality constraint discussed in the next section. This approach prevents estimating parameters that are not resolvable by the data.

The most important feature of our model is not that we pose the problem in terms of stresses, since EHSD results may also be expressed this way [Weertman, 1964], but the fact that our computational domain is no longer an elastic half-space (Figure 1), allowing the evaluation of stress states that are not representable with an EHSD model. The boundaries of our model differ in both geometry and type from those of EHSD models in that they are free surfaces in the absence of applied stresses, while those of an EHSD model are not. Thus, even though it is possible to include a basal boundary in an EHSD model using a second set of dislocations to represent the base, the region below the boundary is still assumed to be completely elastic, which is unlikely to be a reasonable assumption. Plate-like behavior could be simulated with such a model by allowing tensile faults but this does not have a physical analog. In our model we make no explicit assumptions about the material below the overriding plate or the behavior of the subducting slab. We consider only the stresses transmitted to the plate along the fault and through the base. Along the fault, these may represent either frictional or viscous stresses. Along the base they may represent viscous flow in the underlying material or, if we have underestimated the elastic thickness of the plate, they may represent elastic stresses. A difficulty can arise if the elastic thickness of the overriding plate is overestimated since this would invalidate the assumption of elastic behavior throughout the plate. The models in this paper assume elastic behavior throughout the crust. It is possible that the lower crust does not behave elastically and additional modeling will be necessary to determine the effects on both models. Stresses determined by our model represent rates that contribute to observed deformation rates at the surface of the overriding plate, and do not include temporally constant background stresses, so our results will not reflect the absolute stress state. They will indicate how the stresses change over the time period of the measurements,

Copyright 2001 by the American Geophysical Union.

Paper number 2000GL012623.
0094-8276/01/2000GL012623\$05.00

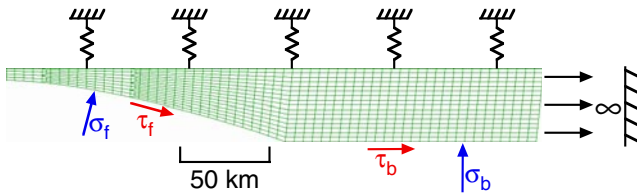


Figure 1. Portion of finite element mesh used in stress computations with applied boundary conditions.

which can help us infer which regions of the fault have moved closer to failure.

3. Application to central Cascadia

We use GPS velocities from 32 sites in northwest Oregon and southwest Washington presented by *McCaffrey et al.* [2000] and supplemented by campaign data collected by us during 2000. As described in that paper in more detail, horizontal site velocities are estimated in the ITRF96 reference frame using the GAMIT/GLOBK software [*King and Bock*, 1999; *Herring*, 1998] and put in the North American (NA) reference frame by removing NA-ITRF96 rotation [*DeMets and Dixon*, 1999]. Since Oregon rotates rapidly about a nearby pole [*McCaffrey et al.*, 2000] we remove the rotational signal in the GPS vectors to isolate the vectors that reveal the plate locking signal (Figure 2). The rotation of Oregon results in much less convergence obliquity at the trench compared to Juan de Fuca-NA motion. We model only trench-normal motion in this study, using the projection of each of the vectors in Figure 2 onto the local normal to the trench. Since formal GPS velocity uncertainties are generally underestimated [*Mao et al.*, 1999], like *McCaffrey et al.* [2000], we multiply them by 3 to compute our χ^2 misfit. We also use two tilt rates near the Oregon coast [*Reilinger and Adams*, 1982] and 1 uplift rate from corrected tide gauge data [*Hyndman and Wang*, 1995]. Tilt rates are assigned at the beginning, middle and end of each line to account for the finite distances over which they were obtained (Figure 2).

The geometry of our model is based on *Hyndman and Wang* [1995] for central Oregon (Figure 1). They show little variation in their profiles between the Columbia River and northern California, approximating a 2D structure. We assume elastic behavior in the overriding plate and frictional behavior on the fault are restricted to the upper 40 km, with shear modulus of 30 GPa and Poisson's ratio of 0.25. We compute equivalent EBSD results using a finite element model and the same inversion scheme. We tried a positivity constraint [*Lawson and Hanson*, 1974] on the shear stress rate along the fault and a loose equality constraint that the horizontal stress on the fault balance the basal shear stress, preventing a net acceleration of the plate. There are thus four constraint permutations: those including positivity but not force balance (P-NFB), neither constraint (NP-NFB), both constraints (P-FB), and force balance and no positivity (NP-FB). Neither constraint is pertinent to an EBSD model. The positivity constraint is not enforceable since, as pointed out by *Douglass and Buffett* [1995], EBSD models will always give rise to both positive and negative shear stress rates along the fault. The force balance constraint is not pertinent since the base of the overriding plate is not explicitly included.

We tried inversions using triangular, Gaussian, step-ramp and Chebyshev functions, and applying various weights to the three components of the fitness function. The results summarized in Table 1 and Figure 3 are those that provided the minimum value of χ_n^2 . The finite plate models provide a better fit to the data than model EBSD regardless of the types of constraints, particularly when vertical data are included. No penalty is incurred by the imposition of shear stress positivity constraints, and very little penalty arises from the force balance constraint. Our preferred model is P-FB, which includes both positivity and force balance constraints. It seems reasonable to expect positive (downdip) shear stress increases from plate motion. If we expect negative shear stress accumulation due to coseismic or long-term aseismic stress relaxation following a large earthquake, for example, model NP-FB or NP-NFB would be a better choice. The force balance constraint is based on the observation that the horizontal surface velocity seems to approach

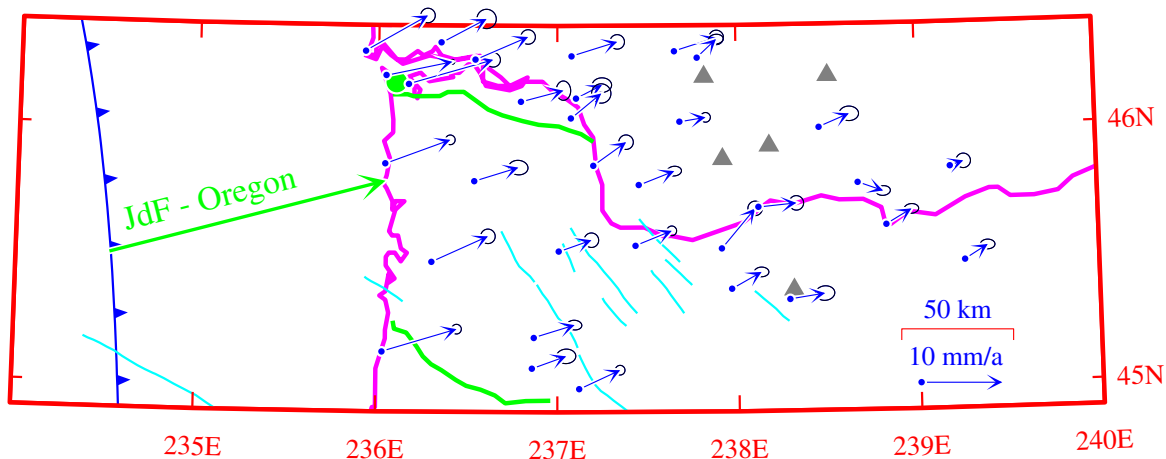


Figure 2. Map view of GPS site velocities relative to NA and associated 3σ error ellipses after removing western Oregon - NA rigid body rotation. The trench-normal component of this velocity field was used in the inversions. Locations of tilt lines are shown with heavy black lines, location of tide gauge station is shown with a black dot, volcanoes are shown with triangles, and NW-trending lines are faults.

Table 1. Values of χ_n^2 for the Different Models

P-NFB	NP-NFB	P-FB	NP-FB	EHSD
0.94 (28)	0.94 (29)	0.99 (27)	0.96 (27)	1.28 (29)
0.79 (34)	0.80 (35)	0.88 (34)	0.84 (33)	1.65 (37)

Number of degrees of freedom shown in parentheses. There are 32 observations for the horizontal data set (first row) and 39 observations for the combined data set (second row), which includes uplift and tilt rates.

zero (Figure 3a) within the computational domain, which extends to 700 km, arguing for a horizontal force balance over the same distance range.

Model P-FB provides an excellent fit to both the horizontal and vertical data (Figures 3a, 3b and 3c). Model EHSD fits the vertical data but has difficulty fitting the change in slope in the horizontal data that begins about 200 km from the trench. This feature crosses the volcanic arc but the fact that it begins far to the west of the arc argues against a magmatic cause. *McCaffrey et al.* [2000] fit this feature by including slip on the fault between 40 and 50 km depth, while *Norabuena et al.* [1998] fit a similar gradual decrease in horizontal velocities in South America by inserting an upper plate fault in their model. Such secondary features are unnecessary with model P-FB, which fits the data by means of a positive shear stress rate within 80 km of the trench, a balancing negative shear stress rate along the portion of the base closest to the trench, and a small positive normal stress rate along the same portion of the base (Figures 3e and 3f). Although the stress rate results in Figure 3 are relatively discontinuous, smoother stress distributions provide a nearly identical fit. The Chebyshev coefficient values in kPa/yr and 1σ uncertainties for model P-FB, with coefficient order in parentheses, are: τ_f , 1.8 ± 0.12 (0); σ_b , -0.62 ± 0.28 (2), 0.28 ± 0.074 (3), -0.16 ± 0.039 (4); τ_b , -0.68 ± 0.045 (0). In general, the relative uncertainties are less for the shear components. For model EHSD, the Gaussian amplitude values are 27.0 ± 2.1 and 8.4 ± 0.84 mm/yr. Figure 3d shows the movement of the upper surface of the fault, which is equal to the movement of the fault plane itself due to the applied dislocations plus one half of the dislocation value. The peak at 90 km for model EHSD represents a region that is nearly locked, with an applied dislocation of about 32 mm/yr. Model EHSD requires at least partial locking all the way to the downdip end of the fault, consistent with the results of *McCaffrey et al.* [2000]. These results are also generally consistent with those of *Hyndman and Wang* [1995], who predict complete locking from 0-60 km and partial locking from 60-120 km for this region. Model P-FB provides a better fit using the stress distribution described above, yielding a smoothly-varying gradient in the upper fault surface velocity that decreases to almost zero at the downdip end. Model P-FB predicts a negative fault-normal velocity at the trench (Figure 3d), resulting in surface subsidence (Figure 3b) that then decreases smoothly to zero far from the trench. Model EHSD predicts a much different pattern with more variation in both velocity components. Although the base of the overriding plate is not explicitly included in model EHSD we are able to compute the shear and normal stress rates along a horizontal plane at 40 km depth (Figures 3e and 3f).

The inferred shear stress rate on the fault may be used to estimate an earthquake stress drop. Great historic subduction earthquakes are thought to have occurred every 400 to 650 years along the southern 2/3 of the Cascadia thrust [*Adams, 1990; Atwater and Hemphill-Haley, 1997; McCaffrey et al., 2000*]. If we assume a recurrence time of 600 years and multiply this by the shear stress rate predicted by model P-FB close to the trench (2 kPa/yr) we obtain a stress drop of about 1.2 MPa, a typical value for an inter-plate earthquake [*Kanamori and Anderson, 1975*]. A similar calculation for model EHSD yields an estimate of about 1.6 MPa for the downdip end of the fault. Model EHSD actually predicts negative (updip) rates of stress accumulation that are greater in magnitude than the positive rates. If interpreted literally, this would indicate coseismic displacement in the opposite (normal) sense from the slip further downdip. This issue has been discussed by *Douglass and Buffett* [1995] in their evaluation of the stress states predicted by dislocation models such as that of *Savage* [1983]. *Savage* [1996] has explained this in terms of a counterbalancing static stress field.

Using estimated stress rates on the fault (Figures 3e and 3f), we compute a Coulomb Failure Function (CFF) rate [*Reasenber and Simpson, 1992*]. We assume that the pore fluid pressure, cohesion, and coefficient of friction do not change significantly over the time period of interest, and that the stress field is superimposed on a preexisting background field of positive (downdip) shear stress. The results of Figure

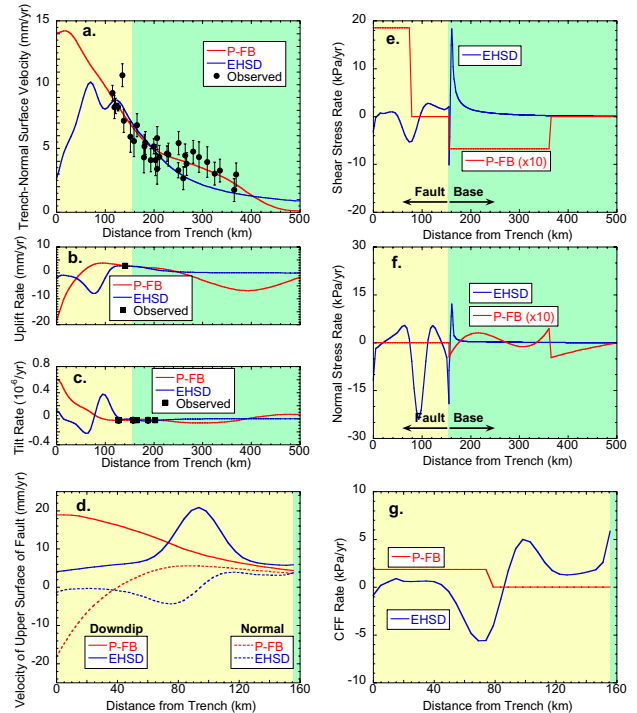


Figure 3. Predicted results for models P-FB and EHSD. (a) Trench-normal component of surface velocity and 3σ uncertainties. (b) Surface uplift rates. (c) Tilt rates. (d) Predicted downdip and fault-normal velocities for the upper surface of the fault. (e) Predicted shear stress rates along the fault and base (results for model P-FB are multiplied by 10). (f) Predicted normal stress rates along the fault and base (results for model P-FB are multiplied by 10). (g) Predicted CFF rates.

3g are based on an assumed coefficient of friction of 0.2, which means that the results will be dominated by the shear stress rate. Model P-FB predicts increased values of CFF rate within 80 km of the trench (offshore), and zero values at greater distances, while model EHSD predicts a much greater variation, with a noticeable peak at 100 km from the trench and positive values to the downdip end of the fault. The peak magnitude is much greater for model EHSD since the stress rates involved are much higher (Figures 3e and 3f). This discrepancy between the two models thus involves not only the pattern, but the magnitude of predicted stress rates.

4. Conclusions

We fit geodetic data from northern Oregon much better using a finite plate model than a half-space dislocation model. The two models make significantly different predictions about the nature of earthquake hazard along the Oregon coast. The plate model predicts that most stress accumulation on the plate-bounding fault occurs close to the trench, and the predicted magnitudes of the stress accumulation rates are significantly smaller than those predicted by a dislocation model. Computed profiles of the CFF rate along the fault are also significantly different for the two models. It may not be advisable to use dislocation models in this sort of calculation, since fault locking does not necessarily correlate with increased values of CFF rate (compare Figures 3d and 3g). Thus, although elastic dislocation models appear to provide a good kinematic description of subduction zone mechanics and coseismic displacement fields, they may not be suitable for investigations of interseismic stress changes.

Acknowledgments. We thank Jim Savage and Kelin Wang for helpful reviews. This work was supported by NSF grant EAR-981496 and USGS-NEHRP-PN1691.

References

Adams, J., Paleoseismicity of the Cascadia subduction zone: Evidence from turbidites off the Oregon-Washington margin, *Tectonics*, *9*, 569-583, 1990.

Atwater, B. F., and E. Hemphill-Haley, Recurrence intervals for great earthquakes of the past 3,500 years at northeastern Willapa Bay, Washington, *USGS Professional Paper 1576*, 1997.

Bettess, P., *Infinite Elements*, 264 pp., Penshaw, Cleadon, Sunderland, 1992.

Carroll, D. L., FORTRAN Genetic Algorithm (GA) Driver, www.staff.uiuc.edu/~carroll/ga.html, 1999.

Curtis, A. and R. Snieder, Reconditioning inverse problems using the genetic algorithm and revised parameterization, *Geophysics*, *62*, 1524-1532, 1997.

DeMets, C. and T. H. Dixon, New kinematic models for Pacific-North America motion from 3 Ma to present, I: Evidence for steady motion and biases in the NUVEL-1A model, *Geophys. Res. Lett.*, *26*, 1921-1924, 1999.

Douglass, J. J., and B. A. Buffett, The stress state implied by dislocation models of subduction deformation, *Geophys. Res. Lett.*, *22*, 3115-3118, 1995.

Herring, T. A., GLOBK: Global Kalman Filter VLBI and GPS analysis program, v.4.1, Mass. Inst. of Technol., Cambridge, 1998.

Hyndman, R. D., and K. Wang, The rupture zone of Cascadia great earthquakes from current deformation and the thermal regime, *J. Geophys. Res.*, *100*, 22,133-22,154, 1995.

Kanamori, H., and D. L. Anderson, Theoretical basis of some empirical relations in seismology, *Bull. Seismol. Soc. Am.*, *65*, 1073-1095, 1975.

King, R. W. and Bock, Y., Documentation for the GAMIT GPS analysis software, Release 9.82, Massachusetts Institute of Technology, Cambridge, 1999.

Lawson, C. L. and R. J. Hanson, *Solving Least Squares Problems*, 340 pp., Prentice-Hall, Englewood Cliffs, 1974.

Mao, A., C. G. A. Harrison, and T. H. Dixon, Noise in GPS coordinate time series, *J. Geophys. Res.*, *104*, 2797-2816, 1999.

McCaffrey, R., M. D. Long, C. Goldfinger, P. C. Zwick, J. L. Nabelek, C. K. Johnson, and C. Smith, Rotation and plate locking at the southern Cascadia subduction zone, *Geophys. Res. Lett.*, *27*, 3117-3120, 2000.

Melosh, H. J. and A. Raefsky, The dynamical origin of subduction zone topography, *Geophys. J. R. Astron. Soc.*, *60*, 333-354, 1980.

Norabuena, E., L. Leffler-Griffin, A. Mao, T. Dixon, S. Stein, I. S. Sacks, L. Ocola, and M. Ellis, Space geodetic observations of Nazca-South America convergence across the central Andes, *Science*, *279*, 358-362, 1998.

Okada, Y., Surface deformation due to shear and tensile faults in a half-space, *Bull. Seismol. Soc. Am.*, *75*, 1135-1154, 1985.

Press, W. H., B. P. Flannery, S. A. Teukolsky, and W. T. Vetterling, *Numerical Recipes, 2nd edition*, 963 pp., Cambridge Univ. Press, Cambridge, 1992.

Reasenber, P. A., and R. W. Simpson, Response of regional seismicity to the static stress change produced by the Loma Prieta earthquake, *Science*, *255*, 1687-1690, 1992.

Reilinger, R., and J. Adams, Geodetic evidence for landward tilting of the Oregon and Washington coastal areas, *Geophys. Res. Lett.*, *9*, 401-403, 1982.

Savage, J. C., A dislocation model of strain accumulation at a subduction zone, *J. Geophys. Res.*, *70*, 4984-4996, 1983.

Savage, J. C., Comment on "The stress state implied by dislocation models of subduction deformation" by J. J. Douglass and B. A. Buffett, *J. Geophys. Res.*, *23*, 2709-2710, 1996.

Weertman, J., Continuum distribution of dislocations on faults with finite friction, *Bull. Seismol. Soc. Am.*, *54*, 1035-1058, 1964.

Williams, C. A. and R. M. Richardson, A rheologically layered three-dimensional model of the San Andreas fault in central and southern California, *J. Geophys. Res.*, *96*, 16,597-16,623, 1991.

Williams, C. A. and G. Wadge, The effects of topography on magma chamber deformation models: Application to Mt. Etna and radar interferometry, *Geophys. Res. Lett.*, *25*, 1549-1552, 1998.

R. McCaffrey and C. A. Williams, Department of Earth and Environmental Sciences, Science Center, Rensselaer Polytechnic Institute, Troy, NY 12180. (e-mail: mccafr@rpi.edu; willic3@rpi.edu)

(Received November 10, 2000; revised March 09, 2001; accepted March 12, 2001.)